

Oscillations of a Flexible Plate Immersed in a Vortex Street

E. Sandoval Hernández and A. Cros

Abstract This experimental study deals with the oscillation of a flexible plate inside the von Kármán street. The flow velocities are much lower than the threshold above which the fluttering instability would develop. The flexible plate is fixed at its leading edge whereas its trailing edge is free. The vortices are detected by tin oxide and the whole system is recorded by a videocamera. We find that the trailing edge of the plate oscillates with a small amplitude and with the same frequency as the incoming vortices. Moreover, the plate wavelength is more than twice the plate length. These results are different from the previous experiments of Allen and Smits (2001) performed with larger plates and at much higher Reynolds numbers. Alben (2010) theoretical study permits to explain these differences.

1 Introduction

A flexible plate can flutter spontaneously in a flow if the flow velocity is high enough. This flutter is due to the aeroelastic instability (Païdoussis 1998) whose mechanism is as follows. The flow generates infinitesimal pressure differences between the two sides of the plate, which provoke plate oscillations. When the flow velocities are lower than a velocity threshold, these oscillations are damped. Nevertheless, above a velocity threshold, the plate oscillations are amplified and the plate flutters with typical spatial shapes and temporal frequencies which depend upon the geometrical and elastic characteristics (Eloy et al. 2008; Michelin et al. 2008).

E. Sandoval Hernández

Natural and Exact Sciences Department CU-Valles, Universidad de Guadalajara,
Carretera Guadalajara—Ameca km. 45.5. C.P., 46600 Ameca, Jalisco, Mexico

A. Cros (✉)

Physics Department CUCEI, Universidad de Guadalajara,
Av. Revolución 1500. Col. Olímpica. C.P., 44430 Guadalajara, Jalisco, Mexico
e-mail: anne@astro.iam.udg.mx

The equation of movement which describes the transversal deflection $y(x, t)$ of the flexible plate in a uniform flow (where x is the axis parallel to the plate chord at rest, t is time and y is the coordinate transversal to the plate area at rest) depends upon the pressure difference Δp between the two faces of the plate. This term is difficult to estimate when it comes from a uniform flow around the plate. In this work a periodic term Δp is set via the von Kármán street.

This experimental study is performed as follows. First a vortex wake is generated behind a cylinder at low Reynolds numbers ($100 < Re < 150$). Then the flexible plate is fixed at its leading edge out of the recirculation region which forms downstream the cylinder, that is at a distance greater than a few cylinder diameters downstream the cylinder. The flexible plate trailing edge is free. We measure the amplitude and the frequency of the free end of the plate as a function of the cylinder diameter and of the Reynolds number, for a fixed plate length. The deflection of the other points along the flexible plate can also be plotted as a function of time. Finally, we compare our results with two previous studies: the experimental work of Allen and Smits (2001) and Alben's (2010) theoretical study.

The paper is organized as follows. In Sect. 2, we present our experimental device. In Sect. 3, we show our results, which are analyzed and discussed in Sect. 4. Conclusion is written in Sect. 5.

2 Experimental Device

The flow is generated in a water channel thanks to a centrifugal pump and controlled via a triphasic frequency converter. Hence, flow velocity can be varied from $v = 0.8$ to 2.0 cm/s with a precision better than 2 %. A 10-cm-long cylindrical obstacle, of two different diameters $D = 5$ and 13 mm, is vertically fixed at the beginning of the test section as illustrated in Fig. 1a. The test section dimensions are $10 \times 10 \times 100$ cm³. The flexible plate is cut from a transparent sheet protector and its elastic and geometrical characteristics are shown in Table 1.

The leading edge of the flexible plate is fixed to a thin metallic wire at the distance $s = 7$ cm downstream the cylinder center, as shown in Fig. 1b. This distance is chosen in such a way that the plate leading edge be outside the suction region behind the cylinder. Besides, the pinned limit condition leads to a natural first frequency in water equal to $f_l \approx 1.2$ Hz.

The visualizations are made by oxidizing a thin tin wire which passes through the flow perpendicularly to the cylinder. One of the extremes of the wire is connected to the negative pole of a power supply while the positive pole is connected to a copper electrode at the end of the test section (Taneda et al. 1977). This visualization method gives better results than the dye method because the vortices appear less deformed when passing near the flexible plate. A photo of the flow and the flexible plate is shown in Fig. 2.

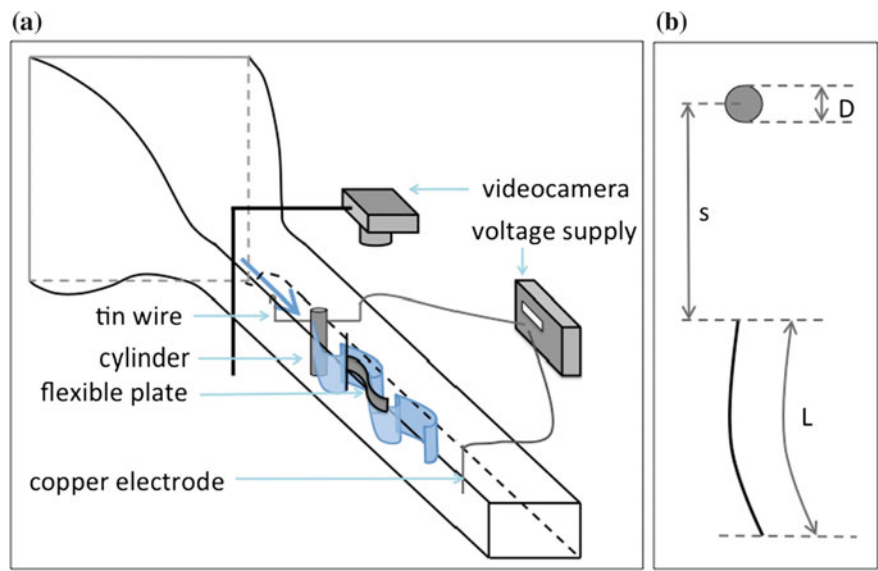


Fig. 1 **a** Experimental set-up. **b** Top view of the system cylinder—flexible plate with the specific distances: the plate length is $L = 6.5$ cm, the cylinder diameters are $D = 5$ and 13 mm, the distance between the plate leading edge and the cylinder center is $s = 7$ cm

Table 1 Geometrical and elastic characteristics of the flexible plate. L is the length, H the height, e the thickness, m_s the mass per unit of area, B the plate flexural rigidity

L (cm)	H (cm)	e (mm)	m_s (g/m ²)	B (N.m)
6.5	2	0.044	34	8.1×10^{-5}

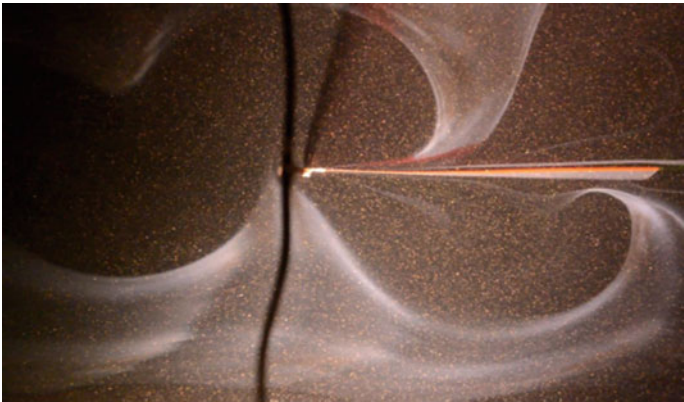


Fig. 2 Photo of the flow around the flexible plate visualized via the tin oxide. The flow goes from *left to right*. The cylinder is not shown in the photo. The *dark vertical line* comes from the support of the flexible plate axis. The vortices are delimited by the tin oxide so that they correspond to the dark regions of the flow

The system {vortices + flexible plate} is recorded thanks to a videocamera (Nikon D5200) placed above the system. The frame size is 1080×1800 pixels, so that the resolution equals to 10 pixels by millimeter.

3 Results

3.1 Influence of the Cylinder Diameter

First, we checked that the flexible plate does not oscillate when it is immersed in the uniform laminar flow generated by the water channel. No oscillation was observed for flow velocities between 0.8 and 2.0 cm/s.

Then, we placed a cylinder with a diameter $D = 5$ mm upstream from the plate. We could not detect any oscillation of the trailing edge of the flexible plate for the same velocity interval.

Finally, the von Kármán street was generated by a cylinder with a diameter $D = 13$ mm. The videocamera could detect a slight oscillation of the free end of the plate. In order to quantify the deflection $y(L, t)$, we performed spatiotemporal diagrams. From each picture of the video we extracted the column of pixels that passes through the free end of the plate. This column is put in the spatiotemporal diagram of Fig. 3 and the same process is repeated for all the pictures. In this way, the x -axis of Fig. 3 is time while the vertical axis represents the space. In the flow, the dark areas correspond to the vortices. It can be observed that the flexible plate oscillates with the same frequency as the von Kármán vortices.

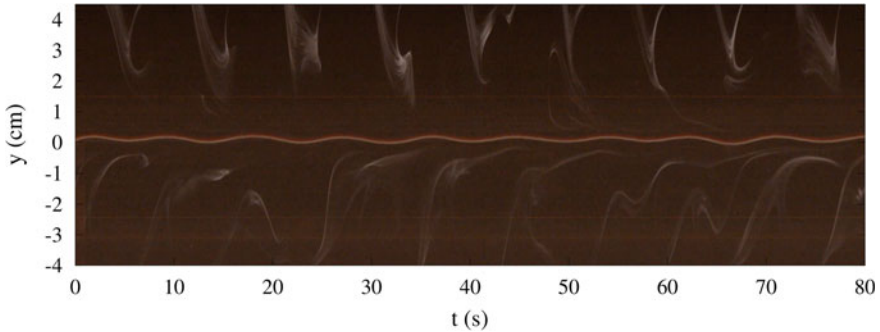


Fig. 3 Spatiotemporal diagram for the cylinder with diameter $D = 13$ mm and $Re = 113$

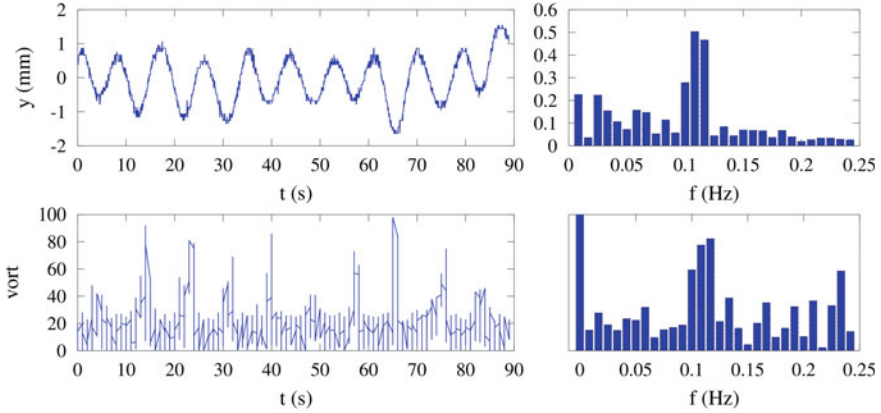


Fig. 4 *Left-hand top plot* temporal evolution of the trailing edge deflection of the plate for $Re = 113$. *Left-hand bottom plot* pixel values of the horizontal line ($y = 3.0$ cm) of the spatiotemporal diagram. *Right-hand plots* respective Fourier spectra

3.2 Influence of the Reynolds Number

We varied the flow velocity v in such a way that the Reynolds number calculated via the obstacle diameter $D = 13$ mm was $Re = [108, 143]$. Several spatiotemporal diagrams were performed and we extracted the trailing edge oscillation, as shown in the left-hand top plot of Fig. 4.

The left-hand bottom plot of Fig. 4 shows the pixel values of the line located at $y = 3.0$ cm in the spatiotemporal diagram. In this plot, the vortices correspond to low values of the pixels (dark areas) while the tin oxide correspond to clearer regions, that is, higher values of the pixels. The right-hand plots are the respective spectra of the left-hand plots. The spectra allow to determine the frequency of the plate and of the vortices for each Reynolds number. These two quantities are plotted in Fig. 5. The red points correspond to the plate trailing edge frequencies while the blue points (generally superimposed with the red points) correspond to the frequency of the von Kármán vortices in presence of the plate. The plain line represents the expected evolution of the vortices frequency as a function of the Reynolds number for the usual von Kármán street given by Fey et al. (1998). This plot means that the presence of the flexible plate does not influence the vortices frequency and that the plate is synchronized with the incoming vortices. Moreover, spatiotemporal diagrams performed at different coordinates of the plate (not shown here) allowed us to conclude that all the points along the plate oscillate with the same phase. That means that the plate wavelength λ is such that $L/\lambda < 0.5$.

Besides, the amplitude A of the plate trailing edge is shown in Fig. 6. It can be seen that A is very small, with a maximum of $A/L \approx 0.01$, equivalent to $A = 0.7$ mm and $A/D \approx 0.05$, at $Re = 140$. This amplitude is much lower than in the Allen and Smits (2001) experiments as discussed next.

Fig. 5 Evolution of the frequencies f of the von Kármán vortices (blue) and the plate trailing edge (red) as a function of Reynolds number Re calculated via the cylinder diameter. The plain line represents the expected frequency of the von Kármán vortices without flexible plate as a function of the Reynolds number (Fey et al. 1998)

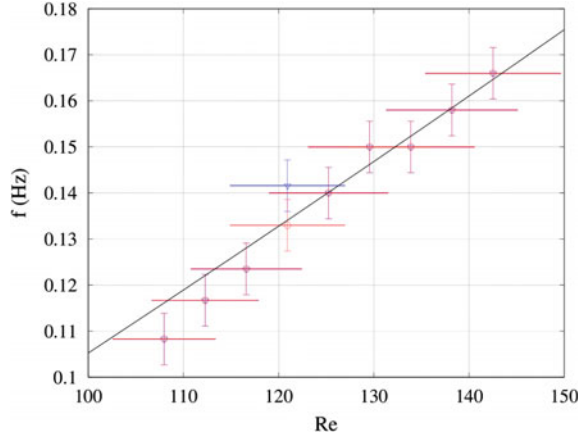
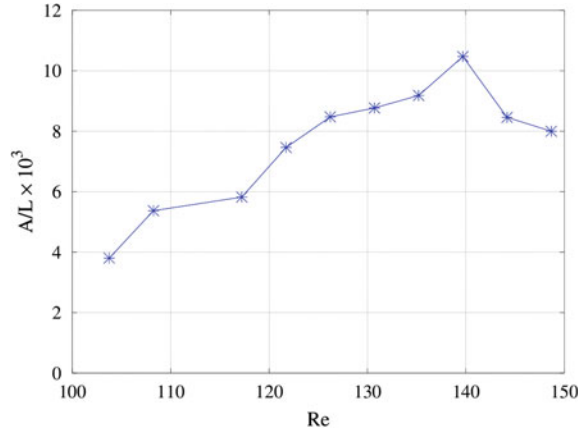


Fig. 6 Evolution of the non-dimensional amplitude A/L of the plate trailing edge as a function of the Reynolds number Re calculated on the cylinder diameter



4 Analysis and Discussion

Allen and Smits (2001) performed the same kind of experiments with plates of different characteristics. In order to compare their plates with ours, the geometrical dimensions, m_s , and B values of their plates are shown in Table 2. We also note that the von Kármán street was generated in their experiments by planar bluff bodies perpendicular to the flow ($D = 5.08$ and 3.81 cm), so that their Reynolds number (calculated via D) varied between 5000 and 40000.

As it can be seen in Table 2, the dimensions and density of their plates are much larger than our plate. As their plate thicknesses are greater too, their flexural rigidities are also higher. The first difference between their observations and our experiments is that their plates oscillate such that $L/\lambda = 1.5 - 2$, where λ is the plate

Table 2 Characteristics of the plates used by Allen and Smits (2001). L is the length, H the height, e the thickness, m_s the mass per unit of area, B the plates flexural rigidity

	L (cm)	H (cm)	e (mm)	m_s (g/m ²)	B (N.m)
18 PVDF	45.7	7.62	0.70	1100	3.1×10^{-3}
24 PVDF	61.0	7.62	0.70	1100	3.2×10^{-3}
18 PU	45.7	7.62	0.60	980	6.1×10^{-4}
18 plastic	45.7	7.62	0.10	200	4.2×10^{-4}

wavelength. This difference can be explained by calculating the wavenumber k^* of the free oscillations of the flexible plate in vacuum. Alben (2010) defines two nondimensional numbers as:

$$R_1 = m_s / \rho L \quad \text{and} \quad R_2 = \frac{B}{\rho v^2 L^3} \left(\frac{l}{L} \right)^2 \quad (1)$$

where ρ is the air density, v the vortex translation velocity and l the vortices wavelength. Alben (2010) defines the nondimensional wavenumber as

$$\frac{k^*}{2\pi} = \frac{1}{\sqrt{2\pi}} \left(\frac{R_1}{R_2} \right)^{1/4} \approx \frac{L}{\lambda}. \quad (2)$$

The order of magnitude of these quantities are shown in Table 3. The value of R_2 is much lower for Allen and Smits (2001) than in our experiment because both their flow velocity and their plate lengths are higher. That is why those authors could observe more than a wavelength along their plate length. It can be seen moreover that the theoretical values of $k^*/(2\pi)$ correspond qualitatively to the observed experimental values L/λ .

Let note that the expression of k^* is also equivalent to the ratio $(\omega_v/\omega_p)^{1/2}$, where $\omega_v = 2\pi v/l$ is the vortex frequency and $\omega_p = [B/(m_s L^4)]^{1/2}$ is a characteristic frequency of the plate. In our case, the vortex frequency ($\omega_v = 0.6 - 1$ rad/s, see Fig. 5) is much lower than the natural frequency of the plate ($\omega_p = 12$ rad/s). In this way, the plate wavelength λ/L is related to the ratio between the natural frequency of the plate and the frequency of the vortices.

The second difference is that Allen and Smits (2001) observed that their plates could reach an amplitude $A = 5D$. This value is much higher than our plate amplitude. Once again, this observation is consistent with the predictions of Alben (2010) who found that the higher R_1 , the greater the amplitude.

Table 3 Order of magnitude of R_1 , R_2 (Eq. 1) and $k^*/(2\pi)$ (Eq. 2) in our experiment and in the Allen and Smits (2001) work

	R_1	R_2	$k^*/(2\pi)$
This study	1×10^{-3}	50–100	0.02
Allen and Smits (2001)	$(0.9-4.8) \times 10^{-3}$	$1 \times 10^{-6}-3 \times 10^{-3}$	0.3–1.5

Finally, in the work of Allen and Smits (2001), when $Re < 10000$, the plates oscillate with a lower frequency than the incoming vortices. They lock on the von Kármán street frequency for high enough flow velocities. In our experiments, we saw that the plate oscillates with the same frequency as the von Kármán vortices for the whole Reynolds interval $Re = [108, 143]$. We think that this is possible thanks to the small oscillation amplitude.

5 Conclusion

In this experimental work, we studied the oscillation of a flexible plate inside von Kármán vortices. The plate has a length $L \approx l$, where l is the wavelength of the incoming vortices. The vortices are generated by a cylinder of diameter D in the interval $Re = [108, 143]$. When $D = 5$ mm, no oscillation is observed. When $D = 13$ mm, we observed that (i) the plate oscillates with the same frequency as the von Kármán vortices and that (ii) the maximum oscillation amplitude is $A/D = 0.05$. Moreover, (iii) our plate oscillates with a wavelength higher than twice the plate length. These observations are different from the results of Allen and Smits (2001), who worked at much higher Reynolds numbers $Re = [5000, 40000]$ and with larger plates. These authors found that (i) their plates reach the same frequency as the von Kármán vortices for high enough Reynolds numbers and that (ii) their plates oscillate with amplitudes that reach $A = 5D$. Moreover, (iii) whereas all the points along our plate oscillate with the same phase, the plates of Allen and Smits (2001) oscillate with a wavelength λ such that $L/\lambda = 1.5 - 2$. These differences are well explained by two nondimensional numbers defined by Alben (2010) which are related to the pressure that the flow exerts on the plate and the mass inertia.

Finally, we comment that, while the objective of Allen and Smits (2001) was to harvest electrical energy from the piezoelectric plate, this kind of experiment is also important to understand how a passive fish can be propelled upstream when placed in von Kármán vortices, as shown by Beal et al. (2006).

Acknowledgements The authors acknowledge the support given by the grant project SEP-CONACyT-2008-103941. A. Cros thanks Stefan Llewellyn Smith for assisting the analysis of the experimental results and Lionel Schouveiler for reviewing the manuscript.

References

- Alben S (2010) Passive and active bodies in vortex-street wakes. *J Fluid Mech* 642:95–125
- Allen JJ, Smits AJ (2001) Energy harvesting eel. *J Fluids Struct* 15(3):629–640
- Beal DN, Hover FS, Triantafyllou MS, Liao JC, Lauder GV (2006) Passive propulsion in vortex wakes. *J Fluid Mech* 549:385–402
- Eloy C, Lagrange R, Souilliez C, Schouveiler L (2008) Aeroelastic instability of cantilevered flexible plates. *J Fluid Mech* 611:97–106

- Fey U, König M, Eckelmann H (1998) A new Strouhal-Reynolds-number relationship for the circular cylinder in the range $47 < Re < 2 \times 10^5$. *Phys Fluids* 10:1547–1549
- Michelin S, Llewellyn Smith SG, Glover BJ (2008) Vortex shedding model of a flapping flag. *J Fluid Mech* 617:1–10
- Païdoussis MP (1998) Fluid–structure interactions, slender structures and axial flow, vol 1. Academic, London, p 572
- Taneda S, Honji H, Tatsuno M (1977) The electrolytic precipitation method of flow visualization. In: *The International symposium on flow visualisation*, pp 133–138

Recent Advances in Fluid Dynamics with Environmental
Applications

Klapp, J.; Sigalotti, L.D.G.; Medina, A.; López, A.;
Ruiz-Chavarría, G. (Eds.)

2016, XIX, 506 p. 342 illus., 226 illus. in color.,
Hardcover

ISBN: 978-3-319-27964-0